BIOCHEMISTRY
including biophysical chemistry & molecular biology
Rapid Report

Biochemistry **2010,** *49,* 5969–5971 5969
DOI: 10.1021/bi100801g

Synchrotron X-ray-Induced Photoreduction of Ferric Myoglobin Nitrite Crystals Gives the Ferrous Derivative with Retention of the O-Bonded Nitrite Ligand†

Jun Yi,‡ Allen M. Orville,§ John M. Skinner,§ Michael J. Skinner,∥ and George B. Richter-Addo*,‡

‡*Department of Chemistry and Biochemistry, University of Oklahoma, 620 Parrington Oval, Norman, Oklahoma 73019,* §*Biology Department, Brookhaven National Laboratory, Upton, New York 11973-5000, and* ∥*High School Research Program, Brookhaven National Laboratory, Upton, New York 11973-5000*

Received May 19, 2010; Revised Manuscript Received June 19, 2010

ABSTRACT: Exposure of a single crystal of the nitrite adduct of ferric myoglobin (Mb) at 100 K to high-intensity synchrotron X-ray radiation resulted in changes in the UV−vis spectrum that can be attributed to reduction of the ferric compound to the ferrous derivative. We employed correlated single-crystal spectroscopy with crystallography to further characterize this photoproduct. The 1.55 Å resolution crystal structure of the photoproduct reveals retention of the O-binding mode for binding of nitrite to the iron center. The data are consistent with cryogenic generation and trapping, at 100 K, of a ferrous d^6 Mb^{II}-(ONO)* complex by photoreduction of the ferric precursor crystals using high-intensity X-ray radiation.

Some mammalian proteins such as the heme-containing myoglobin (Mb) can reduce the nitrite anion (NO_2^-; $pK_a = 3.2$) under hypoxic conditions to nitric oxide (NO) (eq 1) (*1*, *2*) in a process somewhat reminiscent of that employed by denitrifying nitrite reductase (NiR) enzymes.

$$NO_2^- + H^+ + 1e^- \rightarrow NO + OH^- \qquad (1)$$

Although this subject area is under active investigation and debate, Gladwin and co-workers have demonstrated that nitrite protects against myocardial infarction in $Mb^{+/+}$ mice but does not in $Mb^{-/-}$ knockout mice, thus indeed implicating Mb as an in vivo NiR (*1*).

Clearly, the ability of heme to facilitate nitrite reduction (eq 1) necessitates its presence in the ferrous form that can supply the electron needed for this process. We reported the X-ray crystal structure of the related stable ferric d^5 Mb-nitrite compound and showed that the nitrite ligand adopted an O-binding mode [i.e., nitrito (Figure 1)] (*3*). A valid criticism of this reported ferric Mb^{III}-(ONO) structure is that it may not represent the true mode of binding of nitrite to the ferrous Mb just prior to its reduction to NO in vivo. For example, nitrite adopts an N-binding mode in its complex with the ferric Mb H64V mutant (*4*), and this nitro mode was observed in the X-ray crystal structures of the nitrite adducts of cyt cd_1 NiR [*Paracoccus pantotrophus* (*5*)], sulfite reductase hemoprotein [*Escherichia coli* (*6*)], and cyt *c* NiR [*Wolinella succinogenes* (*7*) and *Thialkalivibrio nitratireducens* (*8*)]. In contrast, the nitrito mode was observed in the nitrite adduct of ferric human hemoglobin (*9*).

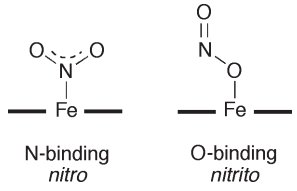

FIGURE 1: Heme nitrite binding modes.

We were unable, however, despite several varied attempts, to generate the physiologically important ferrous d^6 wild-type Mb-nitrite derivative to determine the nitrite binding mode (*3*). We have been intrigued by the use of synchrotron X-ray radiation for the generation of electrons in protein crystals (*10*). We have thus taken advantage of correlated microspectrophotometry and synchrotron X-ray photoreduction techniques to generate and characterize a ferrous d^6 Mb-nitrite compound at 100 K.

Single crystals of ferric horse heart Mb^{III}(ONO) at pH 7.4 were generated as previously described (*3*). The single-crystal UV−vis spectrum of ferric Mb^{III}(ONO) at 100 K is shown in Figure 2A. Exposure of the crystal to low-intensity X-rays (1.0×10^9 photons/s; ~3% of maximal flux) at 100 K at the NSLS that essentially reproduced our "home source" flux (0.7×10^9 photons/s) for 95 min [calculated total X-ray dose of ~0.046 MGy (*11*)] resulted in only a very slight change in the spectrum versus that of the non-X-ray-exposed crystal (Figure 2B). In contrast, exposure of the same crystal of ferric Mb^{III}(ONO) to high-intensity X-rays (3×10^{10} photons/s; $\lambda = 1.0$ Å) at a different locations along the long, narrow, thin plate morphology of the crystal for 50 min (calculated total X-ray dose of ≈0.42 MGy) resulted in rapid and dramatic changes in the optical spectrum (Figure 2C). In particular, the Soret band is red-shifted, and the shape of the bands in the 500−600 nm region undergoes a significant change with the appearance of a relatively intense band at 570 nm. We hypothesized that the changes observed in Figure 2C (i.e., after exposure of the crystal to high-intensity X-rays) were due to the formation and cryotrapping of a six-coordinate ferrous d^6 Mb-nitrite derivative (eq 2, where the asterisk represents X-ray-photoreduced species).

$$Mb^{III}(ONO) + e^- \rightarrow Mb^{II}(ONO/NO_2)^* \qquad (2)$$

Our hypothesis was based on the fact that the spectral changes observed during exposure of ferric Mb^{III}(ONO) (Figure 2C) to high-intensity X-rays at 100 K are very similar to those observed by Schlichting (*10*) and Parak (*12*) when ferric aquometMb underwent X-ray photoreduction at cryogenic temperatures to generate the metastable ferrous $Mb^{II}(H_2O)$ (eq 3 and the

†This work was supported by the Oklahoma Center for the Advancement of Science and Technology (HR9-081, to G.B.R.-A.) and by the Office of Biological and Environmental Research, U.S. Department of Energy, and the National Center for Research Resources (2 P41 RR012408, to A.M.O.) of the National Institutes of Health.

*To whom correspondence should be addressed. Phone: (405) 325-6401. Fax: (405) 325-6111. E-mail: grichteraddo@ou.edu.

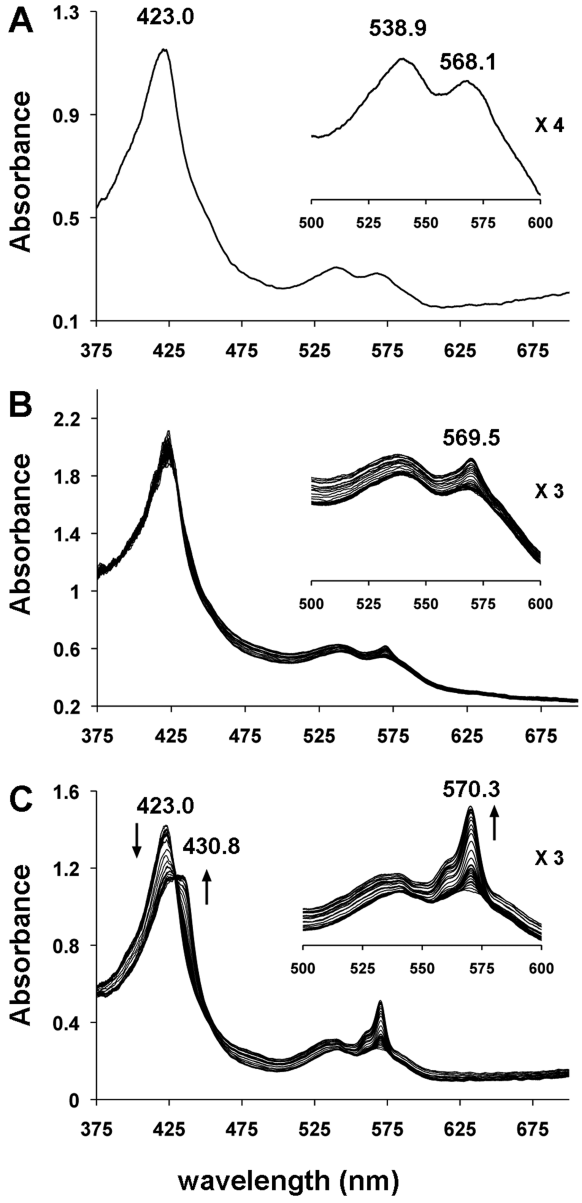

FIGURE 2: Single-crystal UV−vis spectra (~25 μm incident light focal spot size) at 100 K of (A) ferric Mb^{III}(ONO), (B) ferric Mb^{III}(ONO) exposed to low-intensity X-rays over a 95 min period, and (C) ferric Mb^{III}(ONO) exposed to high-intensity X-rays over a 50 min period. In (B) and (C), the first 15 spectra were collected after each image frame (15 s exposure per frame) and the remaining spectra collected after each set of 10 frames.

Supporting Information).

$$Mb^{III}(H_2O) + e^- \rightarrow Mb^{II}(H_2O) \quad (3)$$

To the best of our knowledge, the UV−vis spectrum of authentic ferrous Mb^{II}(ONO) has not been reported. We note, however, that the UV−vis spectrum of the product generated during photoreduction of ferric Mb^{III}(ONO) (eq 2) is also similar to that of the ferrous six-coordinate Mb^{II}(CN) containing an anionic sixth ligand (*13*).

We then turned to correlated spectroscopy−crystallography to identify the products from the exposure of crystals of ferric Mb^{III}(ONO) to low- and high-intensity X-rays. The UV−vis spectrum of a crystal that had been exposed to home source X-ray radiation for data collection is shown on the left in Figure 3; the 1.60 Å resolution crystal structure obtained from the diffraction data [flux of 0.7 × 10^9 photons/s, 0.3 mm beam diameter (Table 1)] is shown on the

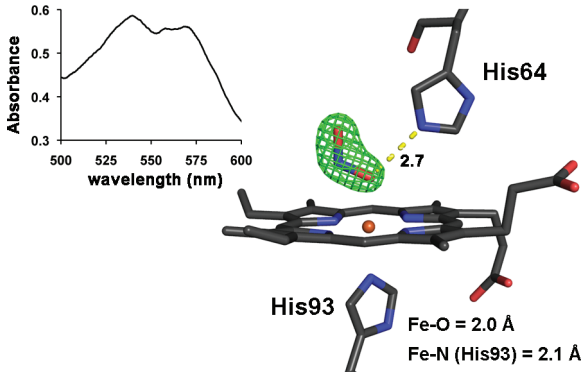

FIGURE 3: Single-crystal optical spectrum (500−600 nm region, ~25 μm incident light focal spot size) of a crystal of ferric Mb^{III}(ONO) after exposure for 12 h to low-intensity home source X-rays. $F_o - F_c$ omit electron density map (contoured at 5σ) and final model of the heme environment of ferric Mb^{III}(ONO) (1.60 Å resolution structure) after exposure to low-intensity home source X-rays. The bonds to Fe have been omitted for the sake of clarity, and the hydrogen bond between the nitrito ligand and the distal His64 residue is shown as a yellow dashed line (distance in angstroms). Protein Data Bank entry 3LR7.

Table 1: Data Collection and Refinement Statistics[a]

	Mb^{III}(ONO)	Mb^{II}(ONO)*
space group	$P2_1$	$P2_1$
wavelength (Å)	1.5418	1.0000
resolution range (Å)	21.85−1.60	26.74−1.55
no. of unique reflections	15927	17892
completeness (%)	98.0 (96.0)	99.2 (95.3)
$I/\sigma(I)$	9.9 (3.0)	15.7 (3.9)
R_{merge} (%)	5.6 (29.8)	4.2 (18.6)
R (R_{free}) (%)	19.3 (24.8)	17.9 (21.2)

[a]The data in parentheses are for the highest-resolution shells.

right. The spectrum confirms that no significant photoreduction occurred during our home source X-ray data collection (cf., Figure 2B). Figure 4 (left) shows the optical spectra of a ferric Mb^{III}(ONO) crystal before (solid line), during (dashed line; after image 161; calculated total X-ray dose of ≈0.45 MGy), and after (gray line; after image 365; calculated total X-ray dose of ≈1.0 MGy) exposure to high-intensity X-rays. Although we collected 365 diffraction image frames (each with 1° oscillation), we used only frames 161−365 for the structure determination because the optical spectra indicated that the product formed during the latter portion of the X-ray exposure was stable. The resulting 1.55 Å resolution crystal structure is shown on the right in Figure 4. Importantly, the UV−vis spectral changes are consistent with photoreduction to the ferrous d^6 Mb^{II}(ONO)* derivative, and the X-ray crystal structure reveals the retention of the O-bound nitrite ligand. This O-binding mode was also observed in a related cobalt-substituted d^6 Co^{III}Mb(ONO) complex (*14*).

The successful generation of a ferrous Mb^{II}(ONO)* complex using high-intensity X-ray radiation may represent a pathway to a nonequilibrium structure in which the O-bonded nitrite is trapped in this position with limited movement in the distal pocket at 100 K. Thus, it may not necessarily represent the true equilibrium structure of the reactive ferrous Mb^{II}-nitrite compound in solution at physiological temperature. Indeed, a similar nonequilibrium retention of the water ligand in X-ray-photoreduced metastable $Mb^{II}(H_2O)$ was obtained at <100 K (*12*); the complex loses its water ligand at temperatures above 150 K to give the well-characterized

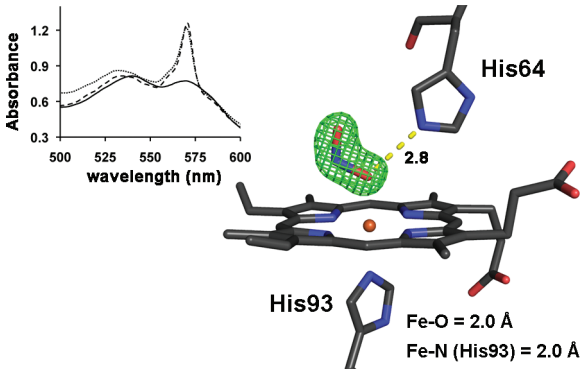

FIGURE 4: Single-crystal optical spectra (500−600 nm region, ~25 μm incident light focal spot size) of a crystal of ferric Mb^{III}(ONO) during exposure to high-intensity X-rays. The dark line is the original spectrum before X-ray exposure. The dashed line is the spectrum after exposure of the crystal to X-rays for 161 images at 15 s/image. The gray line is the spectrum at the end of data collection (365 images at 15 s/image). $F_o - F_c$ omit electron density map (contoured at 5σ) and final model of the heme environment (1.55 Å resolution structure) of the ferrous Mb^{II}-(ONO)* product obtained after exposure of the ferric precursor to high-intensity X-rays using images 161−365 for the structure determination. The bonds to Fe have been omitted for the sake of clarity, and the H-bond between the nitrito ligand and the distal His64 residue is shown as a yellow dashed line (distance in angstroms). Protein Data Bank entry 3LR9. Animations (in avi format) of the correlated crystal rotation spectroscopy have been deposited with the Protein Data Bank and as Supporting Information.

five-coordinate deoxy-Mb form obtained by chemical reduction of ferric $Mb^{III}(H_2O)$. Further, Liu et al. have noted differences in the X-ray crystal structures of *Thermus* cyt ba_3 oxidase reduction products depending on whether X-ray photoreduction or chemical reduction was employed (*15*); the structure of the active site of the X-ray-photoreduced enzyme at 100 K showed retention of the bridging water molecule at the Fe−Cu bimetallic active site, in contrast to the structure of the dithionite-reduced ba_3 that did not show such a bridging water molecule.

In summary, we have successfully generated and cryotrapped a nitrite adduct of ferrous d^6 Mb^{II} at 100 K. This represents the first reported crystal structure of a nitrite adduct of any ferrous mammalian heme protein. Experiments to investigate the thermal stability and reactivity of this Mb^{II}(ONO)* complex are underway.

ACKNOWLEDGMENT

Data for this study were measured, in part, at beamline X26-C of the National Synchrotron Light Source (NSLS) at the Brookhaven National Laboratory. Use of the NSLS was supported by the U.S. Department of Energy Office of Basic Energy Sciences, under Contract DE-AC02-98CH10886. We thank Dr. Timothy Sage for alerting us to ref *12*.

SUPPORTING INFORMATION AVAILABLE

X-ray data collection, structure solution, and refinement and a movie in avi format showing the single-crystal spectra before and after high-intensity X-ray exposure (for the process described in Figure 4) as a function of crystal rotation angle. This material is available free of charge via the Internet at http://pubs.acs.org.

REFERENCES

1. Hendgen-Cotta, U. B., Merx, M. W., Shiva, S., Schmitz, J., Becher, S., Klare, J. P., Steinhoff, H. J., Goedecke, A., Schrader, J., Gladwin, M. T., Kelm, M., and Rassaf, T. (2008) *Proc. Natl. Acad. Sci. U.S.A. 105*, 10256–10261.
2. van Faassen, E. E., Babrami, S., Feelisch, M., Hogg, N., Kelm, M., Kim-Shapiro, D. B., Kozlov, A. V., Li, H. T., Lundberg, J. O., Mason, R., Nohl, H., Rassaf, T., Samouilov, A., Slama-Schwok, A., Shiva, S., Vanin, A. F., Weitzberg, E., Zweier, J., and Gladwin, M. T. (2009) *Med. Res. Rev. 29*, 683–741.
3. Copeland, D. M., Soares, A., West, A. H., and Richter-Addo, G. B. (2006) *J. Inorg. Biochem. 100*, 1413–1425.
4. Yi, J., Heinecke, J., Tan, H., Ford, P. C., and Richter-Addo, G. B. (2009) *J. Am. Chem. Soc. 131*, 18119–18128.
5. Williams, P. A., Fulop, V., Garman, E. F., Saunders, N. F. W., Ferguson, S. J., and Hajdu, J. (1997) *Nature 389*, 406–412.
6. Crane, B. R., Siegel, L. M., and Getzoff, E. D. (1997) *Biochemistry 36*, 12120–12137.
7. Lukat, P., Rudolf, M., Stach, P., Messerschmidt, A., Kroneck, P. M. H., Simon, J., and Einsle, O. (2008) *Biochemistry 47*, 2080–2086.
8. Polyakov, K. M., Boyko, K. M., Tikhonova, T. V., Slutsky, A., Antipov, A. N., Zvyagilskaya, R. A., Popov, A. N., Bourenkov, G. P., Lamzin, V. S., and Popov, V. O. (2009) *J. Mol. Biol. 389*, 846–862.
9. Yi, J., Safo, M. K., and Richter-Addo, G. B. (2008) *Biochemistry 47*, 8247–8249.
10. Beitlich, T., Kuhnel, K., Schultze-Briese, C., Shoeman, R. L., and Schlichting, I. (2007) *J. Synchrotron Radiat. 14*, 11–23.
11. Paithankar, K. S., Owen, R. L., and Garman, E. F. (2009) *J. Synchrotron Radiat. 16*, 152–162.
12. Engler, N., Ostermann, A., Gassmann, A., Lamb, D. C., Prusakov, V. E., Schott, J., Schweitzer-Stenner, R., and Parak, F. G. (2000) *Biophys. J. 78*, 2081–2092.
13. Reddy, K. S., Yonetani, T., Tsuneshige, A., Chance, B., Kushkuley, B., Stavrov, S. S., and Vanderkooi, J. M. (1996) *Biochemistry 35*, 5562–5570.
14. Zahran, Z. N., Chooback, L., Copeland, D. M., West, A. H., and Richter-Addo, G. B. (2008) *J. Inorg. Biochem. 102*, 216–233.
15. Liu, B., Chen, Y., Doukov, T., Soltis, S. M., Stout, C. D., and Fee, J. A. (2009) *Biochemistry 48*, 820–826.